Available online at www.sciencedirect.com

SciVerse ScienceDirect

Proceedings of the Combustion Institute 34 (2013) 929–936

Proceedings of the Combustion Institute

www.elsevier.com/locate/proci

Measurements of the critical initiation radius and unsteady propagation of *n*-decane/air premixed flames

Hwan Ho Kim [a], Sang Hee Won [a,*], Jeffrey Santner [a], Zheng Chen [b,c], Yiguang Ju [a]

[a] *Department of Mechanical and Aerospace Engineering, Princeton University, Princeton, NJ 08544, USA*
[b] *SKLTCS, Department of Mechanics and Aerospace Engineering, College of Engineering, Peking University, Beijing 100871, China*
[c] *SKLTCS, Department of Aeronautics and Astronautics, College of Engineering, Peking University, Beijing 100871, China*

Available online 1 September 2012

Abstract

Unsteady flame propagation, the critical radius for flame initiation, and multiple flame regimes of *n*-decane/air mixtures are studied experimentally and computationally using outwardly propagating spherical flames at various equivalence ratios and pressures. The transient flame speeds, trajectories, and critical radius are measured. The experimental results are compared with direct numerical simulations using detailed high temperature kinetic models. Both experimental and numerical results show that there exist multiple flame regimes in the unsteady spherical flame initiation process. The transition between the flame regimes depends strongly on the mixture equivalence ratio (or Lewis number). It is found that there is a critical flame radius and that it increases dramatically as the mixture equivalence ratio and pressure decrease. The large increase of critical flame radius leads to a dramatic increase of the minimum ignition energy. Furthermore, the flame thickness and the radical pool concentration change significantly during the transition from the ignition flame regime to the self-sustained propagating flame regime. For the same steady state flame speeds, the predicted unsteady flame speeds and the critical flame radius differ significantly from the experimental results. Moreover, different chemical kinetic mechanisms predict different unsteady flame speeds. The existence of multiple flame regimes and the large critical radius of lean liquid fuel mixtures make the ignition of lean mixtures at low pressure and the development of a validated kinetic model more challenging. The unsteady flame regimes, speeds, and critical flame radius should be included as targets of future kinetic model development for turbulent combustion modeling.

Keywords: Critical flame initiation radius; Unsteady flame speed; Flame regimes; High pressure; *n*-Decane

1. Introduction

Understanding of the entire process from flame initiation to propagation is of great importance for successful relight of gas turbine engines [1] and stable operation of the internal combustion engine in unmanned aircraft systems (UAS) [2]. In order to address this issue fundamentally, the flame trajectories of outwardly propagating premixed flames have been investigated in spherical or cylindrical chambers. Theoretical [3], experimental

* Corresponding author.
E-mail address: sangwon@princeton.edu (S.H. Won).

1540-7489/$ - see front matter © 2012 The Combustion Institute. Published by Elsevier Inc. All rights reserved.
http://dx.doi.org/10.1016/j.proci.2012.07.035

[4–6], and numerical [7–9] approaches have shown that the flame undergoes multiple unsteady transitions from initiation to propagation. The unsteady flame transition not only affects the flame initiation period, but also defines a critical flame radius below which ignition might fail [4].

Outwardly propagating flames have been extensively used to determine laminar flame speeds [10–13], but few studies have emphasized unsteady flame transitions [4–6]. A theoretical study examining the unsteady ignition to flame transition was conducted by Chen and Ju [3]. They found that the minimum ignition energy is governed by the critical flame initiation radius, itself a function of the flame chemistry, mixture Lewis number, and flame thickness. The critical flame radius is the radius for spherical flame initiation such that flame kernels that can attain this critical radius result in successful ignition. [7] (see also references in Ref. [7]) In addition, at Lewis numbers less than a critical value (slightly larger than unity), the critical flame initiation radius is dictated by the flame ball size [14]. At Lewis numbers larger than the critical value, the critical flame radius is controlled by the stretch extinction limit. In order to demonstrate the validity of the theoretical study [3], an experimental and numerical study was conducted using hydrogen mixtures in a cylindrical bomb [4]. However, considering that practical systems utilize liquid fuels, it is of interest to quantitatively measure the transient ignition to flame transition, involving the critical flame initiation radius for these fuels.

Jet fuel has an average carbon number of about twelve. Therefore, lean jet fuel/air mixtures have a Lewis number far larger than the critical value. Furthermore, the existence of aromatic components reduces the reactivity, increasing the global activation energy [15,16]. Consequently, the greater Lewis number and activation energy lead to an increased critical radius and minimum ignition energy. Due to difficulties in turbine afterburner and UAS ignition at low pressure [1], it is of interest to investigate the relationship between the critical radius and the success/failure of ignition at low pressure.

Recently, a kinetic model has been developed to quantitatively predict the combustion properties of jet fuel [15,16]. The kinetic model has been validated against laminar flame speeds, but it has not been validated under unsteady conditions. Therefore, the following questions need to be addressed: (1) Can a kinetic model validated by the laminar flame speeds also predict the unsteady flame propagation and the critical radius? (2) How different is the unsteady flame structure from that of the steady flame? (3) How does chemical kinetics affect the unsteady flame propagation? And (4) is this unsteady flame initiation relevant to turbulent combustion?

The goals of the present study are to examine quantitatively the unsteady flame propagation by measuring the critical radius of *n*-decane (n-$C_{10}H_{22}$)/air mixtures at various equivalence ratios and pressures using a near constant pressure spherical bomb. Since *n*-alkane plays a significant role in populating the active radical pool and controlling the high temperature reactivity of jet fuel [15,16], *n*-decane is chosen for the current study. Direct numerical simulations are conducted to assess the fidelity of kinetic models, regarding prediction of flame regimes, critical flame initiation radius, and flame structure.

2. Experimental method and numerical models

The experimental setup is composed of a nearly constant pressure spherical combustion bomb, fuel vaporization chamber, oven, and pressure release system as shown in Fig. 1. The spherical bomb has a 20 cm inner diameter. Two 250 μm diameter tungsten electrodes are installed at the top and bottom of the bomb and the upper electrode is mounted with a linear motion device to control the distance between the electrodes. The bomb is housed inside of an oven heated by two electrical heaters (total 2200 W) with an electric fan to achieve a uniform temperature distribution. K-type thermocouples are installed at the top and bottom of the oven to monitor temperature uniformity. The temperature inside the bomb is maintained at 400 K by PID controller and a K-type thermocouple. The inlet lines and vaporization chamber are also heated to the same temperature as the oven.

The bomb is filled with a combustible mixture using the partial pressure method. *n*-Decane (99% purity) is vaporized in a vaporization chamber (500 cm^3). Nitrogen (99.9%) and oxygen (99.5%) are added to the bomb through heated tubing. A pressure release system is installed for safety [11]. Flame propagation is visualized using a high speed Schlieren imaging [11]. Experimental data for flame radius less than 2.5 cm are used for the analysis to avoid the compression effect [11]. The pressure inside of the bomb rises less than 3%

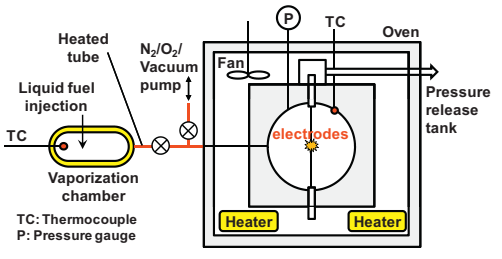

Fig. 1. Schematic of experimental setup.

when the flame radius reaches 2.5 cm, which is the upper limit of all experiments. Therefore, the near constant pressure assumption can be held [9,11]. The confinement effects can be neglected because of the large inner diameter of the spherical bomb, so that the unstretched burned flame speed can be extracted from the linear relationship between burned flame speed and stretch rate $K = (2/R_f) \times (dR_f/dt)$. The laminar flame speed S_u^0 is found by using the calculated equilibrium density ratio.

The experimental uncertainties have been analyzed considering the errors due to pressure readings, temperature fluctuations, mixture concentra tion fluctuations, high-speed visualization, and data analysis. Errors from the Schlieren system were negligible because of the high speed (15,000 fps) and high spatial resolution (86 pixel/cm). The overall uncertainty due to pressure, temperature and mixture fluctuations on laminar flame speed was estimated to be 1.1–7.2% depending on the equivalence ratio using the RMS sum of each uncertainty estimated from [17,18]. The critical radius R_c was determined at the point that the flame trajectory started to deviate from the linear correlation, similar to [4]. The uncertainty in R_c was defined by the radius giving a 1% change in R^2 for the linear correlation between stretch rate and flame speed.

Chemical kinetic models from Chaos et al. [19] and Sirjean et al. [20] are used in calculations. The models are reduced with the Princeton Chem-RC software [21] for computational efficiency. The laminar flame speeds are calculated with CHEMKIN PREMIX [22]. Flame speeds have been calculated up to more than 600 grid points for all flame speed calculations to confirm no dependence on the number of grid points. The comparison between the detailed and reduced models has been made to validate the reduced model.

Unsteady flame propagation is computed using the Adaptive Simulation of Unsteady Reacting Flow (A-SURF-1D) code [9]. The details of the compressible reactive flow governing equations, numerical schemes, initial and boundary conditions, and code validation can be found elsewhere [4,7–9]. In all simulations, the spherical combustion bomb radius is set to be $R_0 = 10$ cm to match the experimental condition. A reflective boundary condition with constant temperature is used at the wall. An initial hot spot with a given radius R_{HOT} and temperature of 1800 K located in the center of the chamber is used to initiate the ignition. In order to match the initial flame trajectories between the experiment and simulation, the size of the ignition hot pocket R_{HOT} is varied between 1 and 3.5 mm. The laminar flame speeds computed from A-SURF with a linear extrapolation are within 4% of PREMIX, justifying the appropriateness of linear extrapolation employed in experiments.

3. Results and discussion

3.1. Laminar flame speeds

The laminar flame speeds have been measured for *n*-decane/air mixtures for equivalence ratio ϕ from 0.7 to 1.4 at initial pressures between 0.7 and 5 atm and the initial temperature, $T_u = 400$ K. Figure 2(a) shows the measured and predicted flame speeds along with published data at atmospheric pressure. For lean mixtures, the measured laminar flame speeds are slightly lower than those from the nonlinear extrapolation of counterflow flames [17], but considerably lower than those from the linear extrapolation using the same configuration [23]. On the rich side, the present measurements are between the two sets of counterflow flame measurements, showing large uncertainty in the measurements of laminar flame speed. Both kinetic models under-predict the laminar flame speeds on the lean side, but exhibit very different predictions on the rich side. At $\phi = 0.9$, however, both models predict the same flame speed as the experiment. This condition will be used later to examine the fidelity of the kinetic models, whether

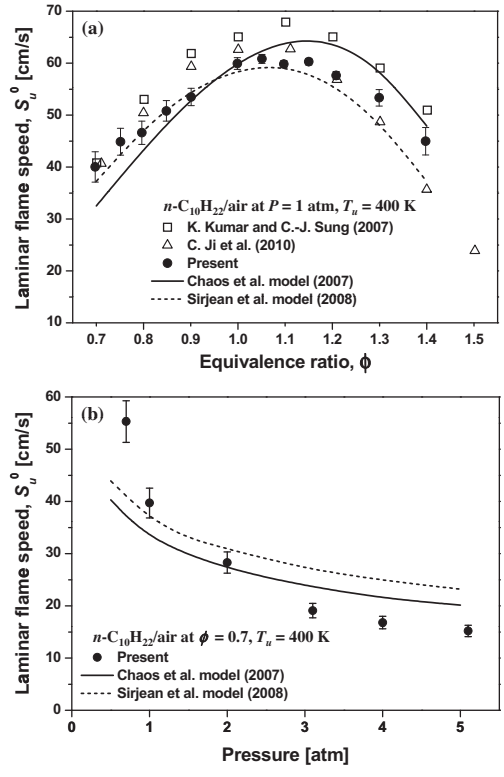

Fig. 2. Experimentally and numerically determined laminar flame speed S_u^0 of *n*-$C_{10}H_{22}$/air mixtures at $P = 1$ atm, $T_u = 400$ K (a), and at $\phi = 0.7$, $T_u = 400$ K (b).

they can predict both laminar and unsteady flame speeds simultaneously.

The laminar flame speeds at pressures from 0.7 to 5 atm for $\phi = 0.7$ are measured and compared with the predictions in Fig. 2(b). The result shows that the laminar flame speed decreases as pressure increases. Note that both models predict the laminar flame speed reasonably well at 1 and 2 atm, but fail to capture the pressure dependence of laminar flame speed in the entire pressure range, indicating the importance of kinetic model validation over a wide range of pressures.

3.2. Observation of three flame regimes

Figure 3(a) and (b) shows the unsteady burned gas flame speed S_b with flame radius and stretch rate, respectively, for $\phi = 0.7$. The result in Fig. 3 (a) shows the existence of three distinct flame regimes; spark assisted ignition kernel propagation (Regime I), unsteady transition from spark ignition to normal flame propagation (Regime II), and normal flame propagation (Regime III). In regime I, the flame speed rapidly decreases with the increase of ignition kernel size right after ignition due to the reduced excess enthalpy from the spark ignition energy. If the ignition energy is lower than a critical value, the ignition kernel will extinguish and ignition will fail [3–5]. The unsteady flame trajectory in regime I strongly depends on the ignition energy [7,8]. If the ignition energy is larger than a critical value, a transition between ignition and flame propagation occurs in regime II. The flame speed in this regime increases rapidly within 2 ms. The fast transition is attributed to a change in flame structure, which will be discussed later with numerical simulations. At the end of regime II, the flame structure becomes close to that of the normal flame. As the flame radius increases and the stretch rate decreases, the normal flame structure approaches that of the unstretched planar laminar flame.

The different flame regimes can be more clearly demonstrated in the stretch rate coordinate in Fig. 3(b). The flame trajectory exhibits two turning points. One represents the transition from regime I to II, and the other from regime II to III. In regime I, the initial kernel development occurs at relatively higher stretch rate from about 200 to 600 s^{-1} with small flame radii. The flame speed decreases with the decrease of stretch due to the ignition energy dissipation. This dependence reconfirms that the ignition kernel propagation is driven by the excess enthalpy from the ignition energy. It takes about 5.7 ms to reach the first turning point. After the first turning point in regime II, the stretch rate has little change due to the simultaneous rapid increases of both the flame radius and the flame speed over 2 ms until the second turning point when the transition to the normal flame occurs.

Figure 4 shows the normalized burned gas flame speed S_b/S_b^0 as a function of K at various equivalence ratios. At $\phi = 0.7$, the flame trajectory exhibits two noticeable turning points, whereas these turning points disappear with richer mixtures. This result clearly shows that the mixture Lewis number, Le, has a significant impact on the unsteady flame trajectories. For rich mixtures at $Le < 1$, stretch strengthens the flame due to the large curvature effect at small flame radius, so the ignition kernel in regime I can directly progress to regime III without experiencing regime II. However for lean mixtures, the flame regime II becomes increasingly important, qualitatively consistent from the theoretical analysis [3].

3.3. Critical flame initiation radius

The dramatic change of flame trajectories has been observed previously with a mixture of large

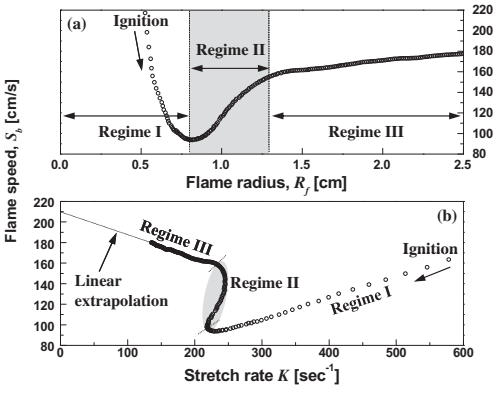

Fig. 3. Flame speed S_b as a function of flame radius R_f (a), and stretch rate K (b) for n-$C_{10}H_{22}$/air at $\phi = 0.7$, $P = 1$ atm, and $T_u = 400$ K.

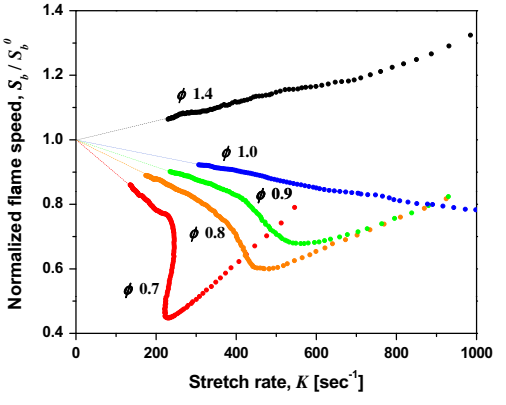

Fig. 4. Normalized flame speed S_b/S_b^0 as a function of stretch rate K for n-$C_{10}H_{22}$/air at $P = 1$ atm and $T_u = 400$ K.

Le such as rich hydrogen/air [4,5], and lean ethanol/air [6] using spherical or cylindrical chambers. Mostly, the normal flames (regime III) have been used to extrapolate the laminar flame speeds. Detailed studies on the other regimes are limited, although Bradley et al. [6] hypothesized the physical meaning of the second turning point as the extinction limit of the premixed flame. It is found that the radius at the minimum flame speed in Fig. 3(a), the first turning point in the present study, is critical for successful ignition [5], but it varies with ignition energy. However, the critical radius is independent from the ignition source when the ignition energy is low [4]. Therefore, the critical radius has been proposed as the radius above which an ignition kernel can lead to a successful ignition (i.e. transition from either regime I or II to III) [3].

Figure 5 shows the experimentally measured and numerically predicted critical radius R_c as a function of equivalence ratio and effective Lewis number, Le_{eff}. The effective Lewis number is a weighted average of the individual fuel and oxidizer Lewis numbers [24]. The critical radius increases rapidly above 10 mm as the equivalence ratio decreases and Le_{eff} increases. Numerical prediction gives a good trend of the equivalence ratio dependence, but fails to predict the quantitative values.

The dependence of the critical radius on pressure for an equivalence ratio of 0.7 is shown in Fig. 6. The critical radius increases rapidly with the decrease of pressure. In general, it has been known that the flame thickness increases as the pressure decreases. This implies that ignition at low pressure will be extremely difficult, thus requires a large ignition energy to overcome the large critical radius. The kinetic model qualitatively predicts the increase of critical radius, but again fails quantitatively.

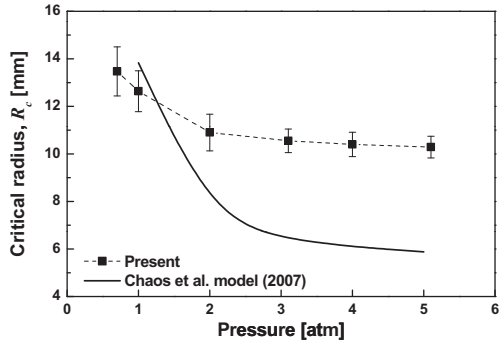

Fig. 6. Critical radius R_c as a function of pressure for n-$C_{10}H_{22}$/air at $\phi = 0.7$ and $T_u = 400$ K.

3.4. Modeling results of unsteady flame trajectory

In order to answer the first question of whether the kinetic model can predict the laminar flame speed and the unsteady flame propagation simultaneously, numerical simulations have been performed with A-SURF [9]. We choose an equivalence ratio of 0.9, at which both models, Chaos et al. [19] and Sirjean et al. [20], reproduce the measured laminar flame speed at $P = 1$ atm and $T_u = 400$ K (Fig. 2(a)). Figure 7 shows both measured and predicted transient flame speed trajectories as a function of stretch rate. Although both models predict the same laminar flame speed, the flame trajectories in regime I and II as well as the critical radius differ significantly from the experimental results and also between the models. To further investigate the impact of ignition energy, the flame trajectories with the Chaos et al. [19] model have been calculated while altering the initial hot pocket size, R_{HOT}, from 2.5 mm to 3.5 mm. The results show that the model accurately predicts the behavior of flame trajectory in regime

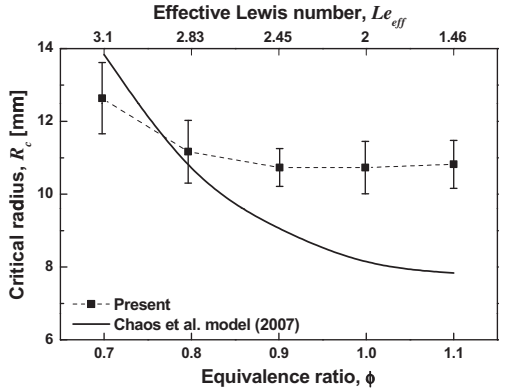

Fig. 5. Critical radius R_c as a function of equivalence ratio and effective Lewis number Le_{eff} for n-$C_{10}H_{22}$/air at $P = 1$ atm and $T_u = 400$ K.

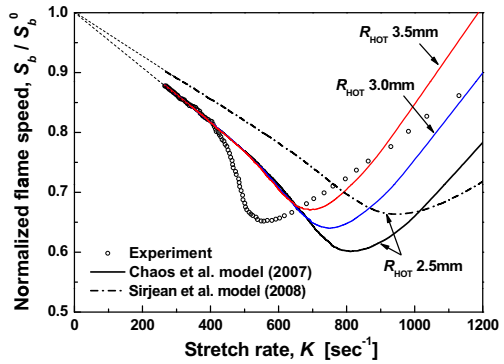

Fig. 7. Experimentally and numerically determined normalized flame speed as a function of stretch rate for n-$C_{10}H_{22}$/air at $\phi = 0.9$, $P = 1$ atm, and $T_u = 400$ K.

III regardless of R_{HOT}, but fails to predict the transitional behaviors in regimes I and II. Although the actual ignition process in the simulation is not identical to the experiment due to spatial nonuniformity and radical deposition in spark ignition, it is noteworthy that two tested kinetic models show different trajectories in the same computational conditions. The models also fail to predict the critical radius and regime III, where the ignition process has no effect on the trajectory for large *Le* mixture. In this regards, the critical radius and unsteady normal flame propagation can be a new validation target of a chemical kinetic model in addition to the laminar flame speed.

As mentioned above, the time duration for regime II is only 2 ms, during which a strong change of flame structure and flame chemistry occurs. Figure 8(c) shows the conditions plotted in Fig. 8(a) and (b) at $\phi = 0.7$. These conditions are given by the first turning point and a point in regime III at the same stretch rate. Figure. 8(b) shows the mole fractions of fuel, ethylene (C_2H_4), H atom, and OH radical at these conditions. The locations of the maximum heat release rates are chosen as the origin of the coordinates. Significant changes in the distributions of heat release rate (HHR) between the two cases are shown in Fig. 8(a) compared to the change of temperature profiles. Considering that the heat release rate in a flame is strongly governed by the rate of radical pool population and its consequent impact on fuel decomposition [25], the result in Fig. 8 indicates the considerable difference in flame chemistry between these two flame regimes. After the energy deposition from the ignition source, the fuel is immediately consumed and a strong radical pool is established. In regime I, the populated radical pool starts to diffuse out, exhibiting the monotonic decay of radical concentration toward the upstream. At the first turning point, point 1 in Fig. 8(c), finally the localized peak of radical concentration appears in the reaction zone, indicating that the flame may be *NOT self-sustained*, but able to overcome the sub-limit strong positive stretch with help from the reduced initial ignition energy. Thus, the time scale between ignition and the first turning point in regime I can be regarded as the delay time for the effect of initial ignition energy and the sub-limit strong stretch, which is a function of ignition energy, mixture Lewis number, and flame chemistry.

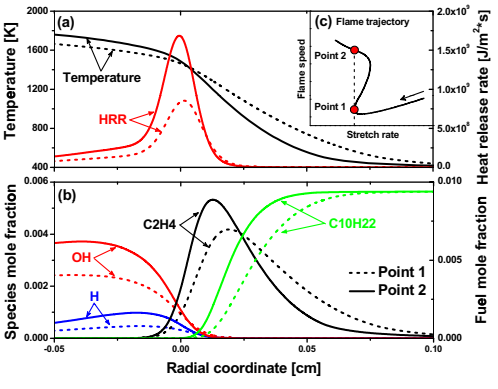

Fig. 8. Flame structures for the first turning point (Point 1) and regime III (Point 2) at stretch rate $K = 210\ \mathrm{sec}^{-1}$: Temperature and heat release rate (a), Species and fuel mole fraction (b), Flame trajectory (c) for n-$C_{10}H_{22}$/air at $\Phi = 0.7$, $P = 1$ atm and $T_u = 400$ K. (the point of maximum heat release rate is shifted to the origin).

Unlike flames in regime I, flames in regime II are *self-sustained* without assistance from the ignition energy. However, the flame is still strongly stretched and has a lower flame temperature due to broadening of the reaction–diffusion zone causing decreased fuel diffusion to the reaction zone. Chemical kinetic flux analyses have been performed to identify the role of chemical kinetics for flames in regime II. The fuel, *n*-decane is mainly decomposed through H abstraction reactions via OH radical, and then converted to C_2H_4 through the sequential unimolecular decomposition reactions [26,27]. C_2H_4 consumption plays an important role in radical pool growth, forming C_2H_3, which leads to production of HCO, CH_2O, and H atoms quickly at high temperature, populating the radical pool (Fig. 8(b)). Consequently, the fuel consumption is promoted by the acceleration of the chain branching reactions, so that the premixed flame structure is fully established by the positive feedback loop of fuel consumption and radical pool growth. The kinetic analysis reconfirmed that flames in regime II are self-sustained.

The changes of the flame trajectory, maximum heat release rate, flame thickness, and maximum mole fractions of key intermediate species are shown in Fig. 9 in the stretch coordinate. These quantities differ dramatically in the different flame regimes. Normalized flame speed shown in Fig. 9(a) qualitatively agrees with experimental result, but differs quantitatively. As the flame in regime II evolves, the flame speed increases and the flame thickness (defined as $(T_{ad} - T_0)/(\max|dT/dx|)$ [28]) decreases, Fig. 9(c). The reduced flame thickness accelerates the diffusion of fuel and further raises the flame temperature, leading to an increase in the radical pool concentration at the transition to regime III. This is why at the same stretch and equivalence ratio, the flame can have different structures. Note that since the flame temperatures and diffusion fluxes of a flame in regime I and II are lower than that of a flame at the same stretch in regime III, the chemical kinetics play different roles in regime I and II compared to that of normal flames.

Both experimental and numerical results in Fig. 9 show that the flame exhibits the unsteady transition (regime II), which can be conceptually regarded as the middle branch in the S-Curve

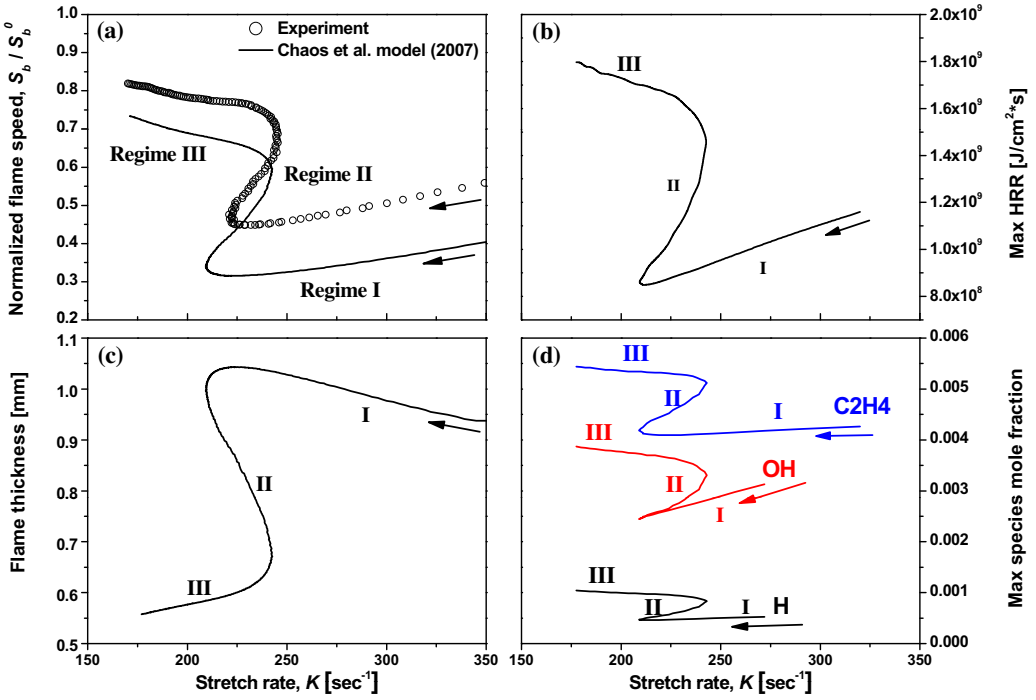

Fig. 9. Normalized flame speed S_b/S_b^0 (a), maximum heat release rate (b), flame thickness (c), and maximum species mole fraction (d) as a function of stretch rate for n-$C_{10}H_{22}$/air at $\Phi = 0.7$, $P = 1$ atm and $T_u = 400$ K.

[29,30]. Classically, the middle branch flame (or weak flame) is often thought unstable. Contrary to the conventional knowledge, the results in Fig. 9 indicate that the weak flame regime can be observed and is an attractor of the unsteady flame propagation. Therefore, the existence of the weak flame and its short evolution time (2 ms) in regime II have an important implication for near limit turbulent combustion where the normal flamelet may not be applicable. Moreover, the big difference in flame structures between regime II and III suggests that the flame trajectories in regime II cannot be used to extrapolate unstretched flame speed either linearly or nonlinearly.

4. Conclusions

The unsteady flame propagation and critical radius of n-decane/air mixtures are measured over a broad range of pressure and equivalence ratio. Three distinct flame regimes, an ignition driven excess enthalpy flame kernel, an ignition to normal flame transition (weak flame), and a normal flame, are observed. There exists a critical radius beyond which a successful flame transition from ignition to normal flame can be achieved. It is found that the mixture equivalence ratio (Lewis number) and the pressure affect the flame regimes and the critical radius. The critical radius increases as the equivalence ratio and pressure decrease, suggesting the possible cause of the ignition difficulty for UAS and afterburner relight.

The weak flame has different flame structures and radical concentrations from that of the normal flame for lean mixtures. The existence of the weak flame and the short transition time suggest that this weak flame regime may be significant in lean, turbulent combustion of large hydrocarbon fuels. Numerical models can reasonably predict the laminar flame speeds but fail to emulate the critical radius and unsteady flame propagation quantitatively. This implies that a kinetic model should be validated against the critical radius and the unsteady conditions for accurate kinetic model development.

Acknowledgement

This work is supported partly supported by the AFRL flame speed research grant with the technical monitor of Barry Kiel and by the Combustion Energy Frontier Research Center, funded by the U.S. Department of Energy, Office of Science, Office of Basic Energy Sciences under Award Number DE-SC0001198. We appreciate the assistance of Tim Bennett and Joe Sivo in constructing the experimental apparatus and also the insightful discussion with Prof. Hai Wang and Dr. Pascal Diévart on the chemical kinetic model.

References

[1] M.B. Colket, S. Zeppieri, H. Hollick, S. Zhang, Fall Technical Meeting: Eastern States Section of the Combustion Institute, Connecticut, 2011, Paper B-02.
[2] J.K. Lefkowitz, Y. Ju, R. Tsuruoka, Y. Ikeda, Fiftieth AIAA ASM, 2012.
[3] Z. Chen, Y. Ju, *Combust. Theory Model.* 11 (2007) 427–453.
[4] Z. Chen, M.P. Burke, Y. Ju, *Proc. Combust. Inst.* 32 (2009) 1253–1260.
[5] A.P. Kelley, G. Jomaas, C.K. Law, *Combust. Flame* 156 (2009) 1006–1013.
[6] D. Bradley, M. Lawes, M.S. Mansour, *Combust. Flame* 156 (2009) 1462–1470.
[7] Z. Chen, M.P. Burke, Y. Ju, *Proc. Combust. Inst.* 33 (2011) 1219–1226.
[8] Z. Chen, *Combust. Flame* 158 (2011) 291–300.
[9] Z. Chen, *Studies on the Initiation, Propagation, and Extinction of Premixed Flames*, Ph.D. thesis, Princeton University, 2008.
[10] B. Lewis, G. von Elbe, *Combustion Flames and Explosive of Gases*, Academic Press, New York, 1961.
[11] X. Qin, Y. Ju, *Proc. Combust. Inst.* 30 (2005) 233–240.
[12] P.D. Ronney, *Opt. Eng.* 33 (1994) 510–521.
[13] C.K. Law, *Combustion Physics*, Cambridge, 2006.
[14] Y.B. Zeldovich, G.I. Barenblatt, V.B. Librovich, G.M. Makhviladze, *The Mathematical Theory of Combustion and Explosions*, Consultants Bureau, New York, 1985.
[15] S. Dooley, S.H. Won, M. Chaos, et al., *Combust. Flame* 157 (2010) 2333–2339.
[16] S. Dooley, S.H. Won, J. Heyne, et al., *Combust. Flame* 159 (4) (2012) 1444–1466.
[17] C. Ji, E. Dames, Y.L. Wang, H. Wang, F.N. Egolfopoulos, *Combust. Flame* 157 (2010) 277–287.
[18] M.P. Burke, M. Chaos, F.L. Dryer, Y. Ju, *Combust. Flame* 157 (2010) 618–631.
[19] M. Chaos, A. Kazakov, Z. Zhao, F.L. Dryer, *Int. J. Chem. Kinet.* 39 (2007) 399–414.
[20] B. Sirjean, E. Dames, D.A. Sheen, et al., A high-temperature chemical kinetic model of *n*-alkane oxidation, JetSurF version 0.2, September 08, 2008 available at http://melchior.usc.edu/JetSurF/Version0_2/Index.html.
[21] W. Sun, X. Gou, Z. Chen, Y. Ju, *Combust. Flame* 157 (2010) 1298–1307, available at http://engine.princeton.edu/.
[22] R.J. Kee, F.M. Rupley, J. Miller, Report No. SAND89-8009B, Sandia National Laboratories, 1989.
[23] K. Kumar, C.-J. Sung, *Combust. Flame* 151 (2007) 209–224.
[24] J.K. Bechtold, M. Matalon, *Combust. Flame* 127 (2001) 1906–1913.
[25] S.H. Won, S. Dooley, F.L. Dryer, Y. Ju, *Combust. Flame* 159 (2012) 541–551.
[26] S.M. Sarathy, C.K. Westbrook, M. Mehl, et al., *Combust. Flame* 158 (2011) 2338–2357.
[27] S. Jahangirian, S. Dooley, F.M. Haas, F.L. Dryer, *Combust. Flame* 159 (2012) 30–43.
[28] C.K. Law, C.J. Sung, *Prog. Energ. Combust.* 26 (2000) 459–505.
[29] F.E. Fendell, *J. Fluid Mech.* 21 (1965) 281–303.
[30] A. Liñán, *Acta Astronaut.* 1 (1974) 1007–1039.